AIMS Materials Science, 12(3): 686–702.
DOI: 10.3934/matersci.2025029
Received: 14 April 2025
Revised: 26 June 2025
Accepted: 14 July 2025
Published: 25 July 2025

http://www.aimspress.com/journal/Materials

Research article

Ex situ synthesis and characterization of chitosan-ZnO nanocomposites using ZnO nanoparticles prepared by the precipitation method

Salah Saleh Habtoor[1,2], Hatijah Binti Basri[2,*], Muhamad Zaini[3], Ainun Rahmawati[3] and Tahir Shah[4]

[1] Department of Chemistry, Faculty of Education, Shabwah University, Yemen
[2] Faculty of Applied Sciences and Technology, Universiti Tun Hussein Onn Malaysia (Pagoh Campus), 84600 Muar, Johor, Malaysia
[3] Nanostructure and Surface Modification Laboratory, Faculty of Mechanical and Manufacturing Engineering, Universiti Tun Hussein Onn Malaysia, 86400 Parit Raja, Batu Pahat, Johor, Malaysia
[4] Applied Science Department, UTAS, PO Box 74, Postal Code 133, Muscat, Oman

* **Correspondence:** Email: hatijah@uthm.edu.my.

Abstract: The varied properties of biopolymer nanocomposites, including their reactive functional groups and nanoscale dimensions, which are not found in bulk materials, have garnered considerable interest for a range of applications. However, their properties and effectiveness are significantly influenced by the synthesis processes employed, as well as the structure and distribution of their components. In this study, the precipitation method was used to prepare zinc oxide nanoparticles (ZnO NPs) at various reaction temperatures. Subsequently, chitosan-zinc oxide nanocomposites (CZ NCs) were synthesized via an ex-situ method, incorporating ZnO NPs with different concentrations of chitosan (CS). Morphological analysis indicated that the size and shape of ZnO NPs were affected by the reaction temperature, with particles synthesized at 40 °C being smaller and exhibiting less aggregation. FTIR analysis of CZ NCs revealed a broad peak at 3312 cm^{-1}, characteristic of the amine and hydroxyl groups present in CS. This peak's shift to a lower wavenumber suggests an interaction between these functional groups and ZnO NPs. Additionally, an absorbance peak at 614 cm^{-1} confirmed the presence of ZnO NPs within the composite. Crystalline analysis showed a reduction in the peak intensity of CZ NCs, attributed to the semi-crystalline nature of CS. Morphological analysis further indicated that the agglomeration of CZ NCs increased with higher concentrations of CS. The distribution of CS molecules within the composite was assessed by evaluating the physical interactions between the CZ NCs and methylene blue (MB) molecules. The sample with 10% chitosan (CS10)

demonstrated a stronger interaction with MB molecules, suggesting a more even distribution of CS throughout the composite. Combining the precipitation method with ex-situ synthesis offers high productivity for nanocomposite production. This approach enables the synthesis of nanocomposites with nanoscale dimensions, which improves the dispersion of active sites and enhances their effectiveness and interaction with other materials. Consequently, these nanocomposites can serve as reinforcements to enhance the properties of various materials.

Keywords: ZnO nanoparticles; biopolymer nanocomposites; functional groups; characterization

1. Introduction

Biopolymer nanocomposites are vital in various fields, including water treatment, food packaging, and medical applications. These materials combine both organic and inorganic substances at the nanoscale, making them versatile for multiple uses [1]. Due to their unique physical and chemical properties, researchers are actively exploring ways to control and enhance these characteristics [2]. Among biopolymers, chitosan (CS) is the second most abundant in nature [3]. It is known for being biodegradable, environmentally friendly, and biocompatible [4].

CS has certain limitations, including low mechanical strength, poor adsorption capacity, reduced chemical stability at high temperatures and pressures, and susceptibility to decomposition in acidic environments [5,6]. To address these issues, CS has been combined with other substances, such as metal oxide nanoparticles [7]. According to Cortes et al., multifunctional materials for various applications are created using CS nanocomposites [8]. CS molecules tend to agglomerate together. This agglomeration diminishes their functional properties, as represented by functional groups [9]. Therefore, selecting the appropriate method for synthesizing CS composites is crucial for obtaining composites with non-agglomerated components and desirable properties.

In biological and environmental applications, it is crucial to prepare non-toxic, chemically stable nanoparticles with unique physical characteristics and high purity for use in the synthesis of biopolymer nanocomposites [10]. It has been demonstrated that metal oxide nanoparticles are non-toxic and have superior chemical stability to metal nanoparticles. Therefore, to produce pure nanoparticles, researchers are turning to simple, low-cost, high-yield techniques that do not require sophisticated equipment.

Zinc oxide nanoparticles (ZnO NPs) possess remarkable physical and chemical properties. The attractive characteristics of ZnO NPs, including their chemical and optical stability, electrochemical coupling coefficient, and radiation absorption capacity, have drawn much attention in recent years [11]. There are numerous ways to produce ZnO NPs, including physical, chemical, and biological techniques [12]. The precipitation method is one of the most promising chemical methods for producing ZnO NPs because it does not require complicated tools or processes and can produce powder on a large scale in straightforward steps [13]. Zinc nitrate and zinc acetate are commonly used as raw materials in the precipitation process for creating ZnO NPs. In addition to controlling the temperature and acidity during the formation of these nanoparticles, reducing agents such as sodium hydroxide and ammonium hydroxide are also utilized. Once the nanoparticles are formed, they are typically washed, dried, and then calcined to produce the final product. One of the main focuses of the research methodology is controlling the size and shape of nanomaterials. These factors determine a material's

properties, which result in a variety of applications [14]. There have been numerous studies carried out to produce ZnO NPs using the precipitation method [15]. A study reported the preparation of ZnO NPs using zinc acetate as a precursor and sodium hydroxide as a reducing agent at various pH levels ranging from 7 to 13. The samples were calcined at 500 °C for 2 h, resulting in the formation of particles with spherical to irregular shapes and non-uniform porous structures [16]. Other researchers synthesized ZnO nanoparticles using the precipitation method, utilizing zinc chloride as a precursor and sodium hydroxide as a reducing agent. The resulting zinc hydroxide was calcined at various temperatures (400–700 °C) in air for 2 h, resulting in nearly spherical particles. The particle size increased with higher calcination temperatures, ranging from 0.11 to 0.5 μm [17]. Zinc nitrate hexahydrate was used as a precursor, and two different reducing agents, sodium hydroxide (NaOH) and potassium hydroxide (KOH), were employed. The calcination process was conducted at 500 °C in a muffle furnace for 3 h. The ZnO NPs exhibited hexagonal shapes when NaOH was the reducing agent, while cylindrical structures were observed when KOH was used [18].

The production of biopolymer nanocomposites has become an important method for applications across various fields due to their diverse uses [19]. Among metal oxide nanoparticles, ZnO NPs, have attracted significant attention in the synthesis of CS nanocomposites. This interest is largely due to their non-toxicity, versatility, and environmental friendliness [20]. However, several factors, such as the type of nanomaterials and the quantity of materials used in the composition, can cause CS molecules to aggregate in the nanocomposite during the reaction process [21]. The functional groups in CS form intermolecular bonds, allowing it to create a supramolecular structure and interact with other materials [22]. The agglomeration of CS molecules can lead to a decrease in the performance of their functional properties. The agglomeration process is significantly affected by the presence of functional groups. Researchers aim to enhance the properties of the composite by ensuring a uniform distribution of CS molecules and by controlling various other factors [23]. Consequently, to synthesize biopolymer nanocomposites with unique characteristics, it is crucial to identify the proper conditions that regulate the synthesis process.

Chitosan-zinc oxide nanocomposites (CZ NCs) are materials that combine ZnO NPs with CS to create composites with improved properties and a wide range of applications [24]. These nanocomposites successfully merge the advantageous characteristics of ZnO NPs, known for their antibacterial and ultraviolet-absorbing properties, with the biodegradable qualities of the CS biopolymer [25].

The ex-situ synthesis of CZ NCs involves the independent preparation of ZnO NPs, which are then incorporated into a CS matrix. These ZnO NPs are typically synthesized using various chemical methods, such as precipitation, hydrothermal, and sol-gel techniques. These methods enable control over the size and shape of the nanoparticles. Once the ZnO NPs are prepared, they are dispersed in a CS solution while continuously stirring to ensure even distribution. A reaction takes place between the ZnO NPs and the functional groups present in CS, leading to the formation of a bio-nanocomposite with enhanced properties. The ex-situ method provides greater control over the properties of nanoparticles before they are integrated into applications. This makes them more suitable for various fields, including medicine, environmental science, and engineering [26]. Additionally, this method helps avoid problems such as incomplete production or the aggregation of nanoparticles that can occur during in situ synthesis.

In this paper, we focus on synthesizing CZ NCs by combining ZnO NPs with varying concentrations of CS. In the first step, ZnO NPs were prepared using the precipitation method. Then,

the ex-situ method was employed to integrate these nanoparticles with different concentrations of CS, allowing for better control over the distribution of CS molecules within the nanocomposite. This technique harnesses the nanoscale space provided by ZnO NPs to distribute CS molecules throughout the composite. Additionally, CS may help in the dispersion and stabilization of ZnO NPs within the composite. The combination of precipitation and ex-situ synthesis methods produces bio-nanocomposites that enhance the dispersion of CS molecules, which contain active sites represented by functional groups, thereby improving their functional properties. These composites can serve various roles, including reinforcement, active components, or support, in materials such as membranes, films, surfaces, and hydrogels. They have applications across medical, engineering, and environmental fields.

The precipitation process requires precise control of parameters to produce nanoparticles suitable for scaling up the production of bio-nanocomposites. This effort aims to prepare ZnO NPs and subsequently blend them with CS matrix using an ex-situ method. The characterization techniques used for the ZnO NPs and CZ NCs include field-effect scanning electron microscopy (FESEM), scanning electron microscopy (SEM), energy-dispersive X-ray spectroscopy (EDS), Fourier transform infrared spectroscopy (FTIR), X-ray diffraction (XRD), and ultraviolet-visible (UV-Vis) spectroscopy.

2. Materials and methods

2.1. Preparation of ZnO NPs

Zinc acetate dihydrate (MW: 219.50 g/mol) (99.68%) and sodium hydroxide pellets (MW: 40.00 g/mol) (98%) were used to produce ZnO NPs. All chemicals were obtained from Sigma Aldrich. ZnO NPs were prepared by the precipitation method. One gram of zinc acetate dihydrate was dissolved in 50 mL of distilled water (solution A), and then 400 mg of sodium hydroxide pellets were dissolved in 50 mL of distilled water (solution B). Furthermore, solution B was completely added dropwise to solution A using magnetic stirring at different reaction temperatures (40–100 °C) for 2 h. The color changed to milky white, and a precipitate was formed during the heating process. The resulting precipitate was separated by centrifugation at 5000 rpm for 20 min and washed three times with distilled water to remove any present impurities. The final sediment was dried in an oven at 60 °C for 8 h and then ground into powder form using a mortar and pestle. Finally, the powder was calcined at 500 °C for 3 h to obtain ZnO NPs.

2.2. Synthesis of CZ NCs

Medium molecular weight chitosan, deacetylated chitin used as an additive biopolymer, and glacial acetic acid (≥99%) are used to dissolve CS. All chemicals were obtained from Sigma Aldrich. CZ NCs synthesized by the ex-situ method according to the work reported by [27], with some modifications as follows: 200 mg of ZnO NPs dispersed in 10 mL of distilled water. CS solutions with different concentrations (5–20% by weight of ZnO NPs) were prepared by dissolving a certain amount of CS in 20 mL of 1% (vol/vol) glacial acetic acid. The CS solution was added to the ZnO NPs solution, and then the mixture was stirred by a magnetic stirrer for 2 h. The product was centrifuged at 5000 rpm and then washed several times with distilled water. The product was dried in an oven at 80 ºC for 24 h.

2.3. Characterization of ZnO NPs and CZ NCs

The results were analyzed to show the properties of the samples using the following equipment: FESEM (JSM-7600F), used to assess the surface morphology of ZnO NPs. SEM (Hitachi SUI5IO) was utilized to identify the surface morphology of CZ NCs. EDS was used to determine which elements make up ZnO NPs and CZ nanocomposites. XRD (Bruker D8 Advance) for the crystallinity of ZnO NPs and confirmation of its integration with CS in the nanocomposite. FTIR (PerkinElmer Spectrum 100) was utilized to confirm the interactions between CZ NCs and ZnO NPs. UV-Vis (Shimadzu UV-1800) was used to assess the methylene blue (MB) dye removal in the aqueous solution through absorption of UV-visible light by MB molecules. The surface morphology of the ZnO NPs and CZ NCs was investigated using FESEM and SEM, respectively. The powdered samples were coated in gold using a gold sputter coater. After that, the samples' surface morphology was examined. The crystal structure of ZnO NPs and CZ NCs is investigated using XRD. The binding of ZnO NPs with the CS matrix, which aids in the formation of CZ NCs, was detected by FTIR. The amount of sample powder was put through FTIR analysis to determine the sample's chemical composition, bonds, and functional groups. The removal of organic dye was examined using UV-Vis. The treated dye solutions were put in cuvette tubes and exposed to UV-Vis light in order to measure how much dye was still present because the dye molecules in the solution absorbed the UV-Vis light.

3. Results and discussion

3.1. Surface morphology of ZnO NPs and CZ NCs

After two hours of reaction at different temperatures, the FESEM results of ZnO NPs samples prepared using the precipitation method show the formation of nanostructured morphologies with various sizes and shapes, as illustrated in Figure 1. The FESEM images reveal that the ZnO NPs vary in size and shape. The figure indicates that as the reaction temperature increases, the particles grow larger and adopt distinct shapes throughout the preparation process of ZnO NPs. Nanoparticles tend to aggregate, leading to distinct shapes and sizes. This variation in size and shape is influenced by the reaction temperature during the preparation of ZnO NPs. Figure 1a shows a FESEM image of ZnO NPs prepared at 40 °C. The prepared ZnO NPs appear well-dispersed, with no noticeable aggregates. The nanoparticles are arranged in small conical and spherical structures. Their size is smaller compared to the other samples, which is noteworthy. Due to their small dimensions, there are gaps between the nanoparticles, increasing their surface area accessibility. In the image shown in Figure 1b, the ZnO NPs prepared at 60 °C appear as irregularly shaped particles. They are distributed in flower-like nanostructures, with some smaller spherical shapes also present. These nanoparticles are larger than those depicted in Figure 1a because they are formed from smaller units. In other words, the smaller nanoparticles aggregate to form larger, diverse nanostructures during nanoparticle formation at this temperature. Furthermore, Figure 1c illustrates that the ZnO NPs prepared at 80 °C appear as asymmetric spindles surrounded by smaller particles. They grow in two dimensions on an irregular nanostructure, unlike the shape of the nanoparticles shown in Figure 1b.

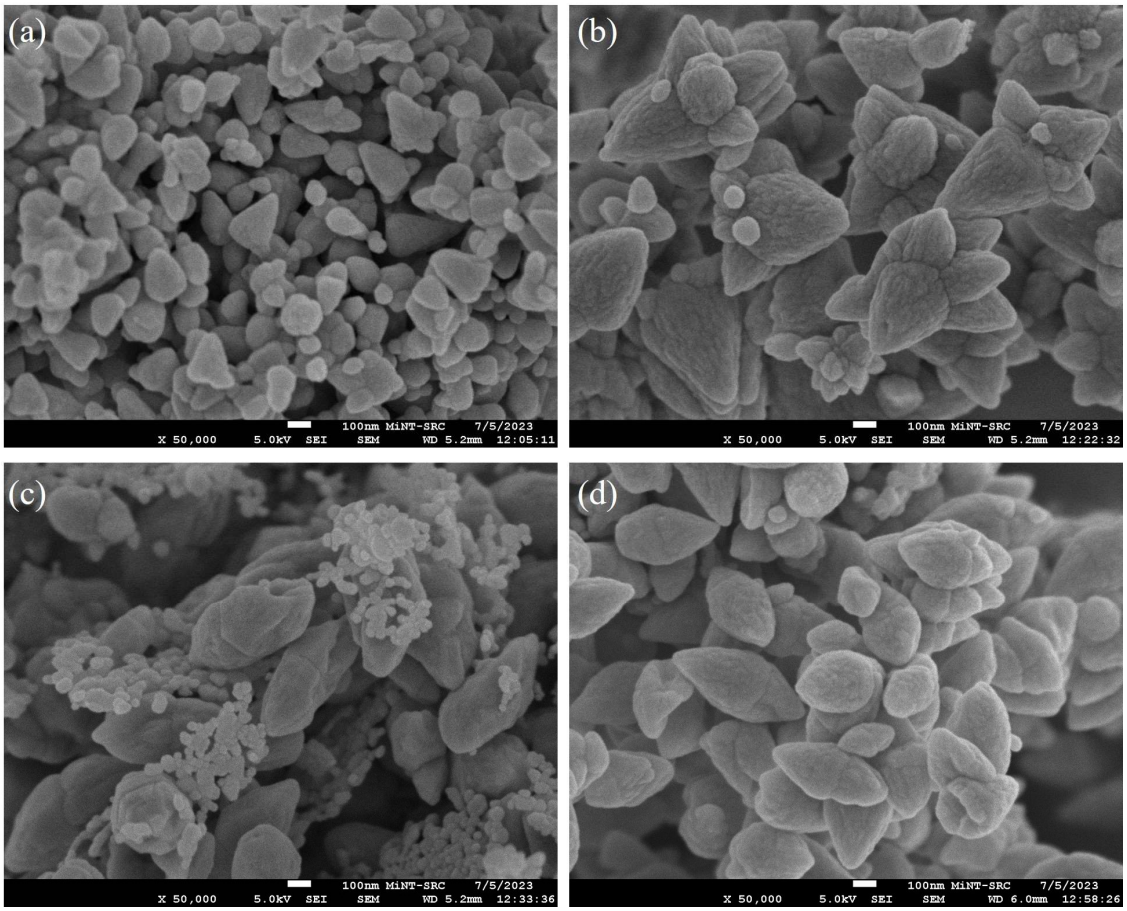

Figure 1. FESEM image of ZnO NPs synthesized at different reaction temperatures: (a) 40 ℃, (b) 60 ℃, (c) 80 ℃, and (d) 100 ℃.

Concerning the ZnO NPs prepared at 100 °C, Figure 1d illustrates that these particles are more widely distributed and possess a spindle shape. Despite having two nano dimensions, these nanoparticles are more uniform and evenly distributed compared to those shown in Figure 1c. It is anticipated that the increase in reaction temperature contributes to the improved regularity of these nanoparticles. It is clear that as the temperature decreases during the preparation of ZnO NP, the size of the nanoparticles diminishes, leading to a more uniform distribution. Lower temperatures can help reduce the agglomeration of ZnO NPs produced through the precipitation method. At this stage, the goal is to obtain smaller ZnO NPs to facilitate their use in the next step, which involves synthesizing a biopolymer nanocomposite by combining nanoparticles with biopolymer molecules. Additionally, small-sized nanoparticles demonstrate advantages over larger ones. The ZnO NPs depicted in Figure 1a are smaller than the other nanoparticles, as indicated by the surface morphology results. This smaller size suggests that they possess a larger surface area compared to the other nanoparticles. Therefore, these nanoparticles have been selected for use in the next stage of synthesizing the biopolymer nanocomposite.

Figure 2 shows the EDS spectrum of the prepared ZnO NPs, while Table 1 presents the corresponding findings. The table reports the atomic percentages and weights of the detected elements, which include oxygen and zinc. The presence of carbon may be due to acetate residues from the sample preparation process. Additionally, gold was used to coat the sample to enhance conductivity during examination.

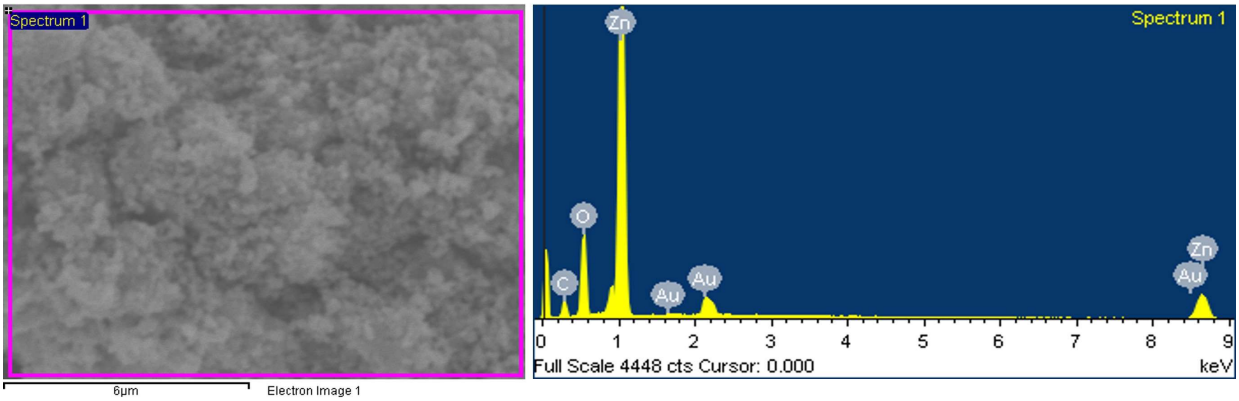

Figure 2. EDS image of ZnO NPs synthesized at 40 °C

Table 1. Elemental composition for the synthesized ZnO NPs at 40 °C

Element	Weight (wt%)	Atomic (%)
O	22.06	53.62
Zn	77.94	46.38
C	10.87	29.17
Au	8.54	1.40

The surface morphology of CZ NCs produced using the ex-situ method is shown in Figure 3 through SEM analysis. This figure illustrates the surface morphology of pure CS as well as its integration with ZnO NPs. In Figure 3b,c, ZnO NPs are evenly dispersed throughout the composite, while in Figure 3a, they are absent in pure CS. The ZnO NPs are evenly distributed throughout the composite along with the CS molecules, as shown in Figure 3b. This combination enables the ZnO NPs to impart nanoscale dimensions to the CS molecules [28]. In Figure 3c, the composite appears flatter and shows agglomerated ZnO NPs on its surface. This agglomeration occurs due to the increased concentration of CS molecules, which causes them to aggregate within the composite. ZnO NPs offer greater opportunities for CS molecules to interact with them through intermolecular bonds during the synthesis process [29]. This interaction helps stabilize the ZnO NPs and ensures they are evenly distributed along the polymer chain within the CS matrix. As a result, the properties of the composite are enhanced due to the symmetrical arrangement of the ZnO NPs and the CS chain. Our goal of this research is to synthesize a nanocomposite with well-distributed and stabilized components that do not agglomerate. Improved distribution of the functional groups in the CS molecules throughout the composite ultimately enhances the functional properties of the composite. Ex-situ synthesis of CZ NCs with controlled CS concentrations prevents agglomeration, which can cause the composites to lose their properties.

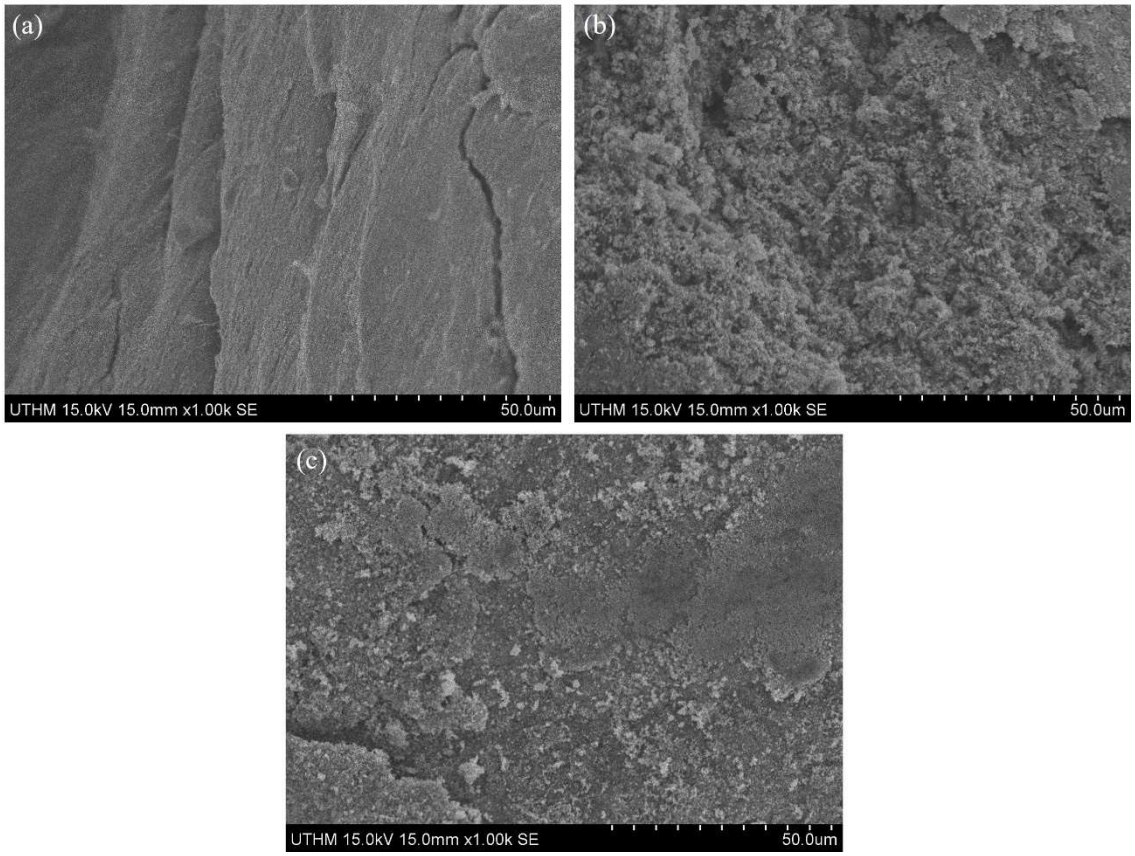

Figure 3. SEM image of the (a) pure chitosan; (b) CZ nanocomposite (10 wt%); and (c) CZ nanocomposite (20 wt%).

Figure 4 shows the quantitative and qualitative composition of the components that make up the nanocomposite, as determined by EDS analysis. In Figure 4a, the presence of peaks for oxygen and zinc is identified, which corresponds to the pure ZnO NPs discussed in the first stage. Figure 4b displays peaks for carbon, oxygen, and nitrogen, indicating the presence of pure CS. The combination of zinc, oxygen, carbon, and nitrogen in Figure 4c represents the CZ NCs, suggesting that ZnO NPs have been combined with CS molecules. The results of the EDS analysis for the CZ NCs synthesized using the ex-situ method are summarized in Table 2.

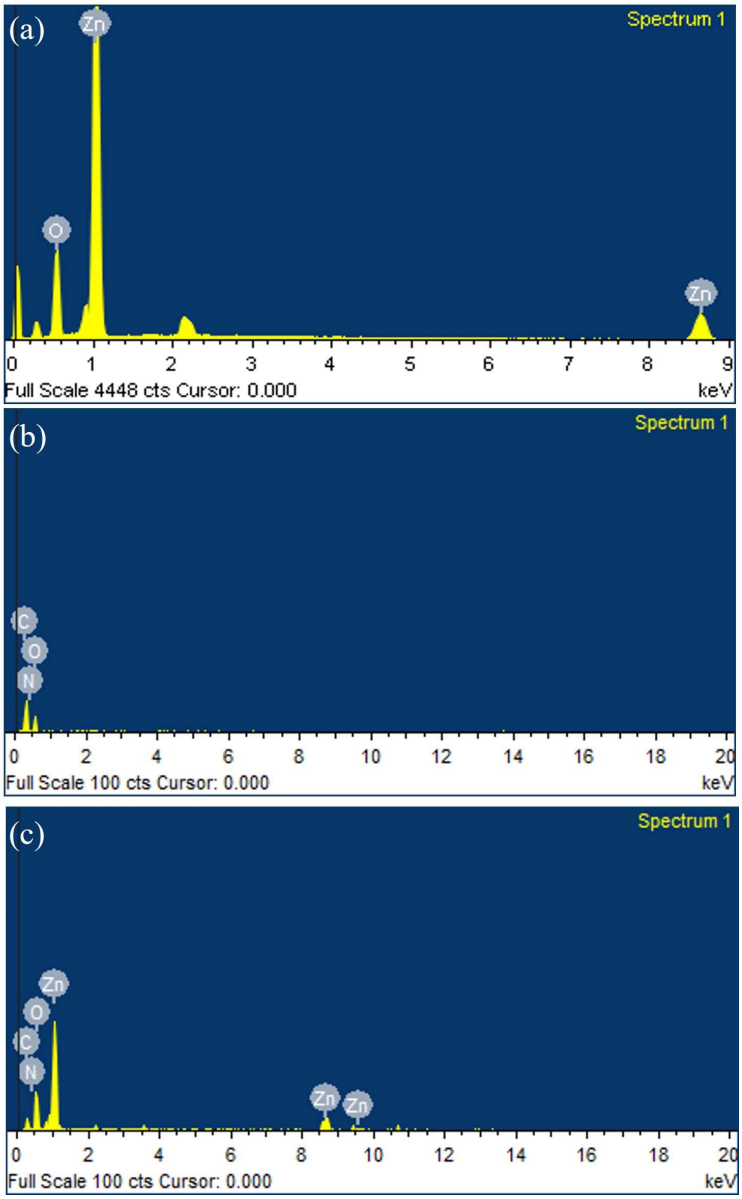

Figure 4. EDS image of (a) ZnO NPs; (b) chitosan; and (c) synthesized CZ nanocomposite.

Table 2. Elemental composition for the synthesized CZ nanocomposite, ZnO NPs, and chitosan.

Sample	Element	Weight (wt%)	Atomic (%)
ZnO	O	22.06	53.62
	Zn	77.94	46.38
CS	C	42.10	48.30
	N	14.95	14.71
	O	42.95	37.00
CZ	C	15.21	32.17
	N	5.11	9.27
	O	23.03	36.55
	Zn	56.65	22.01

3.2. FTIR of ZnO NPs and CZ NCs

Figure 5 shows the FTIR spectra of pure CS, CZ NCs, and ZnO NPs. FTIR analysis was conducted to determine the chemical composition of CS, ZnO NPs, and CZ NCs, which aids in understanding the formation of CZ NCs and the interaction mechanism between ZnO NPs and the CS matrix. The figure displays three distinct FTIR absorption patterns: One for pure CS, one for ZnO NPs, and one for CZ NCs. In the CS spectrum, a broad peak at 3428 cm^{-1} corresponds to the stretching vibrations of hydroxyl (–OH) and amino ($–NH_2$) groups. The peaks at 2854 and 2923 cm^{-1} represent the stretching vibrations of C–H bonds. The bending vibration of the amino group is indicated by the absorption peak at 1650 cm^{-1}, while the deformation of the amide contributes to the absorption peak at 1592 cm^{-1}. Additionally, the stretching vibrations of the C–O bonds are associated with the peaks at 1064 and 1023 cm^{-1}. These findings are consistent with a previous study that utilized the in-situ method to synthesize the CS-ZnO nanocomposite [30].

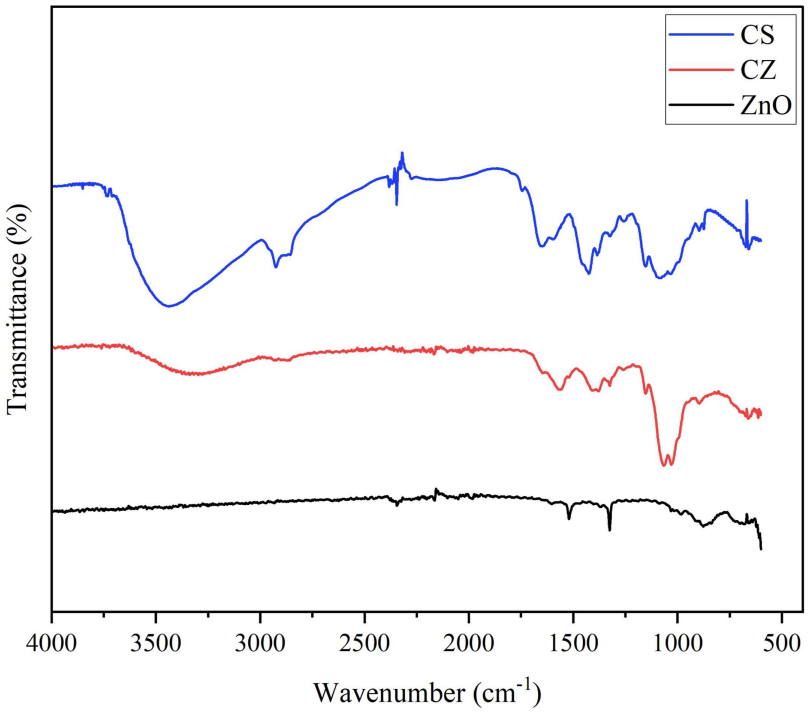

Figure 5. FTIR spectra of the synthesized CZ nanocomposite, ZnO NPs, and pure chitosan.

The absorption peaks at 1088 and 1421 cm^{-1} are associated with C–O stretching and CH_2 bending vibration, respectively [31]. The asymmetric stretching of the C–O–C bridge is responsible for the absorption peak at 1385 cm^{-1}, while the symmetric deformation of CH_3 is responsible for the peak at 1151 cm^{-1} [32]. The C–N bond's stretching vibration is represented by the peak at 1254 cm^{-1} [33]. There are five major absorption peaks in the 500–4000 cm^{-1} range of the ZnO NPs absorption spectrum. The bending vibration of absorbed CO_2 in the air is responsible for the peaks in the absorption range of 2400–2300 cm^{-1} [34]. The symmetrical and asymmetrical stretching of the carboxylate is responsible for the peaks seen at 1520 and 1325 cm^{-1}, respectively [35]. The peak identified as belonging to the stretching vibration of Zn–O is between 875 and 500 cm^{-1} [36,37]. A broad absorption peak that is less intense than the CS peak and shifted towards a lower wavenumber at 3297 cm^{-1} is

visible when the CZ NCs spectrum is compared to the pure CS and ZnO NPs spectra. This shows that ZnO NPs' interaction with the functional groups in the CS matrix creates hydrogen bonds between the oxygen atom in the zinc oxide and the proton in the amine group in the CS [38]. The stretching of Zn–O is responsible for the appearance of a new absorption peak at 614 cm^{-1} [39]. This suggests that ZnO NPs have been incorporated into the CS chain.

3.3. XRD of ZnO NPs and CZ NCs

The crystalline structure of ZnO NPs, CZ NCs, and CS was investigated by XRD, as shown in Figure 6. The XRD pattern of ZnO NPs shows several very sharp and intense peaks. These peaks align perfectly with the hexagonal wurtzite crystal of zinc oxide (JCPDS File No. 36-1451) and are consistent with typical ZnO NPs.

The zinc oxide planes (100), (002), (101), (102), (200), (112), (201), (004), and (202) were assigned to the peaks that were discovered at 31.78, 34.44, 36.26, 47.54, 56.58, 62.84, 66.28, 67.94, 69.02, 72.54, and 76.88°, respectively [40]. The high purity of the prepared ZnO NPs was demonstrated by the absence of any additional peaks caused by impurities. The crystalline state of the hydrate (form 1 and form 2) is responsible for the two low peaks in the CS XRD pattern, which are at 22.3 and ≈20°, respectively [41]. According to this, CS is semi-crystalline. The XRD pattern of CZ NCs is consistent with that of ZnO NPs (JCPDS No. 36-1451), and the findings were published [42,43]. This is due to the interaction of ZnO NPs with the CS matrix [44]. The pattern shows a decrease in the peak intensity of the CZ nanocomposite compared to the peak intensity of the ZnO NPs. This indicates an increase in amorphous components due to the presence of CS, which has semicrystalline properties [45].

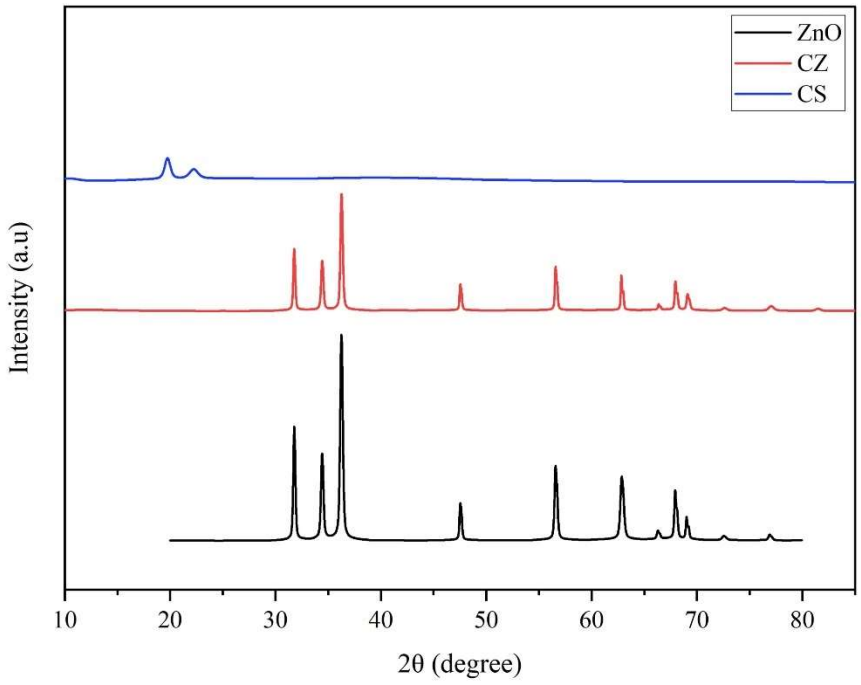

Figure 6. XRD pattern of pure chitosan, synthesized CZ nanocomposite, and ZnO NPs.

3.4. Interactive properties of CZ NCs

The interaction efficiency of CZ NCs with organic molecules was investigated using the dye removal of MB dye molecules. The interaction of MB dye molecules with the active sites of CS molecules on the surface of CZ NCs in aqueous solution using UV-Vis spectra was used to measure the dye removal using CZ NCs synthesized at various CS contents (5, 10, 15, and 20 wt%), as illustrated in Figure 7.

The absorption intensities of the various samples of MB dye solutions treated with CZ NCs were measured to observe the dye removal process. Several UV-Vis spectra of samples treated with CS5, CS10, CS15, and CS20 are displayed. The absorbance of the MB dye, which serves as a control, is responsible for the highest absorption peak at 664 nm. The analysis showed a difference in the samples' absorption intensities compared to the control, indicating that the ZnO NPs arranged the CS molecules in the composite [46]. This is because the functional groups in the CS molecules can interact physically with the MB dye molecules. The lower absorption intensity in sample CS10 indicates that the CS molecules interacted with the MB molecules in the solution more than in samples CS5, CS15, and CS20 because they are more widely distributed with the ZnO NPs. This shows the distribution of CS molecules and their non-agglomeration in the nanocomposite, which enhances their functional properties. Solutions treated with CS15 and CS20 displayed high absorption intensities due to reduced interaction between the nanocomposites and the dye molecules. This indicates that the CS molecules started to aggregate, leading to fewer interaction sites. CS5 exhibits high absorbance intensity due to a lower integration of CS molecules with the ZnO NPs, indicating the nanocomposite has fewer functional groups compared to the CS10 sample. This results in reduced interaction capability with MB molecules.

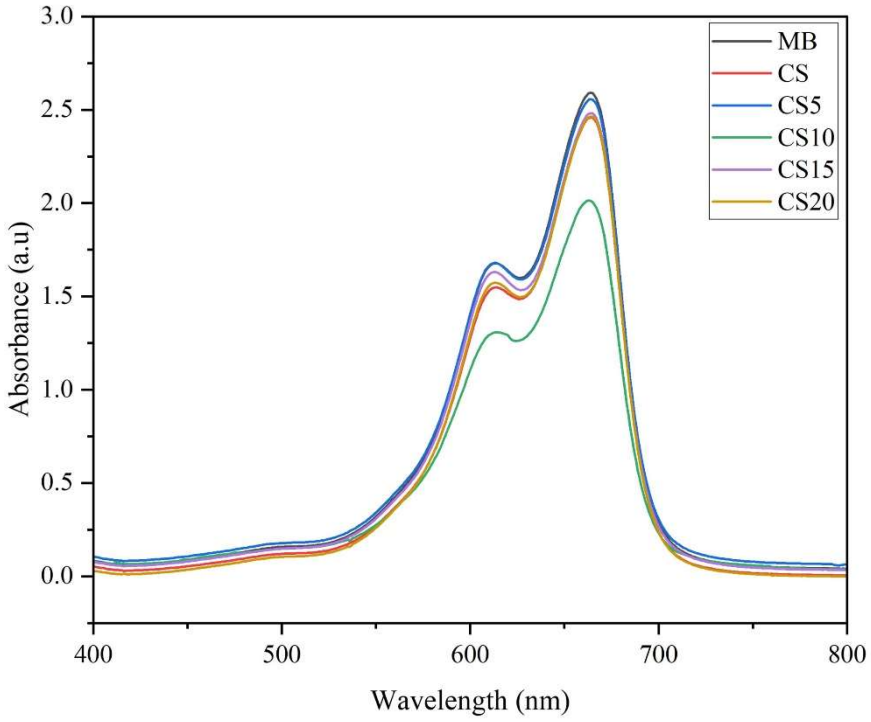

Figure 7. UV-Visible absorption spectra of removal of MB by CS and the synthesized CZ nanocomposite at different contents of chitosan (5, 10, 15, and 20 wt%).

4. Conclusions

Biopolymers offer immense potential due to their biocompatibility and sustainability, making them highly applicable across various fields and opening new avenues for advancements in medicine, environmental science, engineering and materials science. In this study, ZnO NPs were successfully prepared using the precipitation method. We explored the effect of temperature on their size and shape, observing distinct morphological structures including conical, flower-like, and spindle-shaped forms as the reaction temperature increased from 40 to 100 °C. Furthermore, CZ NCs were successfully synthesized at various CS concentrations using the ex-situ method. The analysis confirmed the successful incorporation of CS molecules with the ZnO NPs, demonstrating that the ZnO NPs facilitated a wide distribution of CS molecules and were effectively stabilized within the CS matrix. However, an increase in CS concentration within the nanocomposite led to the agglomeration of CS molecules, which consequently reduced the number of active sites and, thus, the removal efficiency of MB molecules. The controlled precipitation method for ZnO NPs and the ex-situ synthesis of CZ NCs allowed for the creation of uniformly distributed biopolymer nanocomposites. These bio-nanocomposites possess numerous active sites and diverse functionalities, highlighting their promising applications.

Use of AI tools declaration

The authors declare that no artificial intelligence tools were used in the creation of this article.

Acknowledgement

The research facilities were supported by Universiti Tun Hussein Onn Malaysia (UTHM) through the Multi-Disciplinary Research Grant (Q720). Authors also thank the Nanostructures and Surface Modification Laboratories, Faculty of Mechanical and Manufacturing Engineering, Universiti Tun Hussein Onn Malaysia.

Author contributions

Salah Saleh Habtoor drafted the manuscript, conducted the experiments, and collected the data. Hatijah Binti Basri developed research ideas, supervised data analysis, and reviewed the literature. Muhamad Zaini prepared the samples. Ainun Rahmawati interpreted the research results. Tahir Shah contributed to the research methodology and manuscript editing. All authors reviewed and approved the final manuscript.

Conflict of interest

The authors declare no conflict of interest.

References

1. Nandhini J, Karthikeyan E, Rajeshkumar S (2024) Eco-friendly bio-nanocomposites: Pioneering sustainable biomedical advancements in engineering. *Discover Nano* 19: 86. https://doi.org/10.1186/s11671-024-04007-7
2. Phadtare P, Viswapriya V, Shinde V, et al. (2024) Hybrid bionanocomposites as the advancements in biomedical utility. *Hybrid Adv* 8: 100365. https://doi.org/10.1016/j.hybadv.2024.100365
3. Priyadarshi R, Rhim JW (2020) Chitosan-based biodegradable functional films for food packaging applications. *Innovative Food Sci Emerging Technol* 62: 102346. https://doi.org/10.1016/j.ifset.2020.102346
4. Qamar SA, Ashiq M, Jahangeer M, et al. (2020) Chitosan-based hybrid materials as adsorbents for textile dyes—A review. *Case Stud Chem Environ Eng* 2: 100021. https://doi.org/10.1016/j.cscee.2020.100021
5. Vakili M, Rafatullah M, Salamatinia B, et al. (2014) Application of chitosan and its derivatives as adsorbents for dye removal from water and wastewater: A review. *Carbohydr Polym* 113: 115–130. https://doi.org/10.1016/j.carbpol.2014.07.007
6. Liu J, Rojas-Andrade MD, Chata G, et al. (2018) Photo-enhanced antibacterial activity of ZnO/graphene quantum dot nanocomposites. *Nanoscale* 10: 158–166. https://doi.org/10.1039/C7NR07367D
7. Dos Santos JM, Pereira CR, Pinto LAA, et al. (2019) Synthesis of a novel $CoFe_2O_4$/chitosan magnetic composite for fast adsorption of indigotine blue dye. *Carbohydr Polym* 217: 6–14. https://doi.org/10.1016/j.carbpol.2019.04.054
8. Cortés YZ, Valenzuela LM, Peña EAE, et al. (2021) Antibacterial activity of electrospun nanocomposites fabricated by in situ chitosan/silver nanoparticles. *IEEE Trans NanoBiosci* 21: 89–96. https://doi.org/10.1109/TNB.2021.3092287
9. Aranaz I, Mengíbar M, Harris R, et al. (2009) Functional characterization of chitin and chitosan. *Curr Chem Biol* 3: 203–230. https://doi.org/10.2174/187231309788166415
10. Nikzamir M, Akbarzadeh A, Panahi Y (2021) An overview on nanoparticles used in biomedicine and their cytotoxicity. *J Drug Delivery Sci Technol* 61: 102316. https://doi.org/10.1016/j.jddst.2020.102316
11. Kołodziejczak-Radzimska A, Jesionowski T (2014) Zinc oxide—From synthesis to application: A review. *Materials* 7: 2833–2881. https://doi.org/10.3390/ma7042833
12. Patel M, Mishra S, Verma R, et al. (2022) Synthesis of ZnO and CuO nanoparticles via sol gel method and its characterization by using various technique. *Discover Mater* 2: 1. https://doi.org/10.1007/s43939-022-00022-6
13. Zueva SB (2018) Current legislation and methods of treatment of wastewater coming from waste electrical and electronic equipment processing, In: Vegliò F, Birloaga I, *Waste Electrical and Electronic Equipment Recycling*, Cambridge: Woodhead Publishing, 213–240. https://doi.org/10.1016/B978-0-08-102057-9.00009-3
14. Djalali R, Samson J, Matsui H (2004) Doughnut-shaped peptide nano-assemblies and their applications as nanoreactors. *J Am Chem Soc* 126: 7935–7939. https://doi.org/10.1021/ja0319691
15. Sharma P, Hasan MR, Mehto NK, et al. (2022) 92 years of zinc oxide: has been studied by the scientific community since the 1930s—An overview. *Sens Int* 3: 100182. https://doi.org/10.1016/j.sintl.2022.100182

16. Mechai F, Al Shboul A, Bensidhoum MO, et al. (2024) Influence of pH on room-temperature synthesis of zinc oxide nanoparticles for flexible gas sensor applications. *Chemosensors* 12: 83. https://doi.org/10.3390/chemosensors12050083
17. Saidani A, Boudraa R, Fendi K, et al. (2024) Effect of calcination temperature on the photocatalytic activity of precipitated ZnO nanoparticles for the degradation of rhodamine B under different light sources. *Water* 17: 32. https://doi.org/10.3390/w17010032
18. Gines-Palestino RS, Montalvo-Romero C, Solano GL, et al. (2024) Microstructural, morphological, and optical study of synthesis of ZnO and Pt ZnO nanoparticles by a simple method using different precipitating agents. *J Braz Chem Soc* 35: e-20230092. https://doi.org/10.21577/0103-5053.20230092
19. Abdellaoui H, Bouhfid R, Qaiss A (2017) Preparation of bionanocomposites and bionanomaterials from agricultural wastes, In: Jawaid M, Boufi S, HPS A, *Cellulose-Reinforced Nanofibre Composites*, Cambridge: Woodhead Publishing, 341–371. https://doi.org/10.1016/B978-0-08-100957-4.00015-2
20. Yao KX, Zeng HC (2007) ZnO/PVP nanocomposite spheres with two hemispheres. *J Phys Chem C* 111: 13301–13308. https://doi.org/10.1021/jp072550q
21. Ali H, Ismail AM (2022) Recyclable and biodegradable Ag@chitosan nanocomposite beads synthesized in one-step for catalytic hydrogenation of 4-nitrophenol. *J Polym Environ* 30: 3379–3390. https://doi.org/ 10.1007/s10924-022-02441-1
22. Strnad S, Zemljič LF (2023) Cellulose–chitosan functional biocomposites. *Polymers* 15: 425. https://doi.org/10.3390/polym15020425
23. Jamarun N, Prasejati A, Zulhadjri Z, et al. (2024) Effect of chitosan concentration on hydroxyapatite/chitosan composite synthesis using the *in-situ* method as a dye adsorbent. *Kuwait J Sci* 51: 100252. https://doi.org/10.1016/j.kjs.2024.100252
24. Preethi S, Abarna K, Nithyasri M, et al. (2020) Synthesis and characterization of chitosan/zinc oxide nanocomposite for antibacterial activity onto cotton fabrics and dye degradation applications. *Int J Biol Macromol* 164: 2779–2787. https://doi.org/10.1016/j.ijbiomac.2020.08.047
25. Bharathi D, Ranjithkumar R, Chandarshekar B, et al. (2019) Preparation of chitosan coated zinc oxide nanocomposite for enhanced antibacterial and photocatalytic activity: As a bionanocomposite. *Int J Biol Macromol* 129: 989–996. https://doi.org/10.1016/j.ijbiomac.2019.02.061
26. Kachare KS, Shendage SS, Vhanbatte SB, et al. (2024) Synthesis, characterization, and antibacterial study of chitosan–zinc oxide nanocomposite-coated superhydrophobic cotton fabric. *RSC Adv* 14: 33774–33783. https://doi.org/10.1039/D4RA05950F
27. Nguyen NT, Nguyen NT, Nguyen VA (2020) *In situ* synthesis and characterization of ZnO/chitosan nanocomposite as an adsorbent for removal of congo red from aqueous solution. *Adv Polym Technol* 2020: 3892694. https://doi.org/10.1155/2020/3892694
28. Tabassum Z, Girdhar M, Kumar A, et al. (2023) ZnO nanoparticles-reinforced chitosan–xanthan gum blend novel film with enhanced properties and degradability for application in food packaging. *ACS Omega* 8: 31318–31332. https://doi.org/10.1021/acsomega.3c03763
29. Moura D, Mano JF, Paiva MC, et al. (2016) Chitosan nanocomposites based on distinct inorganic fillers for biomedical applications. *Sci Technol Adv Mater* 17: 626–643. https://doi.org/10.1080/14686996.2016.1229104

30. Prokhorov E, Luna-Bárcenas G, Yáñez Limón JM, et al. (2020) Chitosan-ZnO nanocomposites assessed by dielectric, mechanical, and piezoelectric properties. *Polymers* 12: 1991. https://doi.org/10.3390/polym12091991
31. Mahalakshmi S, Hema N, Vijaya PP (2020) *In vitro* biocompatibility and antimicrobial activities of zinc oxide nanoparticles (ZnO NPs) prepared by chemical and green synthetic route—A comparative study. *BioNanoSci* 10: 112–121. https://doi.org/10.1007/s12668-019-00698-w
32. Queiroz MF, Teodosio Melo KR, Sabry DA, et al. (2014) Does the use of chitosan contribute to oxalate kidney stone formation? *Mar Drugs* 13: 141–158. https://doi.org/10.3390/md13010141
33. Gu Z, Xie H, Huang C, et al. (2013) Preparation of chitosan/silk fibroin blending membrane fixed with alginate dialdehyde for wound dressing. *Int J Biol Macromol* 58: 121–126. https://doi.org/10.1016/j.ijbiomac.2013.03.059
34. Muthukumaran S, Gopalakrishnan RJ (2012) Structural, FTIR and photoluminescence studies of Cu doped ZnO nanopowders by co-precipitation method. *Opt Mater* 34: 1946–1953. https://doi.org/10.1016/j.optmat.2012.06.004
35. S Yadav R, Mishra R, C Pandey A (2009) Particle size distribution study by small-angle X-ray scattering technique and photoluminescence property of ZnO nanoparticles. *J Exp Nanosci* 4: 139–146. https://doi.org/10.1080/17458080902929937
36. Bashir S, Awan MS, Farrukh MA, et al. (2022) *In-vivo* (Albino Mice) and *in-vitro* assimilation and toxicity of zinc oxide nanoparticles in food materials. *Int J Nanomed* 17: 4073. https://doi.org/10.2147/IJN.S372343
37. El Faroudi L, Saadi L, Barakat A, et al (2023) Facile and sustainable synthesis of ZnO nanoparticles: Effect of gelling agents on ZnO shapes and their photocatalytic performance. *ACS Omega* 8: 24952–24963. https://doi.org/10.1021/acsomega.3c01491
38. Wang X, Du Y, Yang J, et al. (2006) Preparation, characterization and antimicrobial activity of chitosan/layered silicate nanocomposites. *Polymer* 47: 6738–6744. https://doi.org/10.1016/j.polymer.2006.07.026
39. Vaidehi D, Bhuvaneshwari V, Bharathi D, et al. (2018) Antibacterial and photocatalytic activity of copper oxide nanoparticles synthesized using *Solanum lycopersicum* leaf extract. *Mater Res Express* 5: 085403. https://doi.org/10.1088/2053-1591/aad426
40. Patterson AL (1939) The Scherrer formula for X-ray particle size determination. *Phys Rev* 56: 978. https://doi.org/10.1103/PhysRev.56.978
41. Kumar-Krishnan S, Prokhorov E, Ramírez M, et al. (2014) Novel gigahertz frequency dielectric relaxations in chitosan films. *Soft Matter* 10: 8673–8684. https://doi.org/10.1039/C4SM01804D
42. Muraleedaran K, Mujeeb VA (2015) Applications of chitosan powder with *in situ* synthesized nano ZnO particles as an antimicrobial agent. *Int J Biol Macromol* 77: 266–272. https://doi.org/10.1016/j.ijbiomac.2015.03.058
43. Rahman PM, Mujeeb VA, Muraleedharan K, et al. (2018) Chitosan/nano ZnO composite films: Enhanced mechanical, antimicrobial and dielectric properties. *Arabian J Chem* 11: 120–127. https://doi.org/10.1016/j.arabjc.2016.09.008
44. Hezma AM, Rajeh A, Mannaa MA, et al. (2019) An insight into the effect of zinc oxide nanoparticles on the structural, thermal, mechanical properties and antimicrobial activity of Cs/PVA composite. *Colloids Surf A* 581: 123821. https://doi.org/10.1016/j.colsurfa.2019.123821
45. Fideles TB, Santos JL, Tomás H, et al. (2018) Characterization of chitosan membranes crosslinked by sulfuric acid. *Open Access Libr J* 5: 1–13. https://doi.org/10.4236/oalib.1104336

46. Mokhtar A, Abdelkrim S, Djelad A, et al. (2020) Adsorption behavior of cationic and anionic dyes on magadiite-chitosan composite beads. *Carbohydr Polym* 229: 115399. https://doi.org/10.1016/j.carbpol.2019.115399

AIMS Press